PAPER • OPEN ACCESS

Limitations in artificial spin ice path selectivity: the challenges beyond topological control

To cite this article: S K Walton *et al* 2015 *New J. Phys.* **17** 013054

View the article online for updates and enhancements.

New Journal of Physics

The open access journal at the forefront of physics

CrossMark

PAPER

Limitations in artificial spin ice path selectivity: the challenges beyond topological control

S K Walton[1], K Zeissler[1], D M Burn[1], S Ladak[2], D E Read[2], T Tyliszczak[3], L F Cohen[1] and W R Branford[1]

1 Blackett Laboratory, Department of Physics, Imperial College, Prince Consort Road, South Kensington, London SW7 2AZ, UK
2 School of Physics and Astronomy, Cardiff University, Queens Buildings, The Parade, Cardiff CF24 3AA, UK
3 Advanced Light Source, Lawrence Berkeley National Laboratory, MS 6-2100 Berkeley, CA 94720, USA

E-mail: W.branford@imperial.ac.uk

Abstract

Magnetic charge is carried through nanowire networks by domain walls, and the micromagnetic structure of a domain wall provides an opportunity to manipulate its movement. We have shown previously that magnetic monopole defects exist in artificial spin ice (ASI) and result from two bar switching at a vertex. To create and manipulate monopole defects and indeed magnetic charge in general, path selectivity of the domain wall at a vertex is required. We have recently shown that in connected ASI structures, transverse wall chirality (or topology) determines wall path direction, but a mechanism known as Walker breakdown, where a wall mutates into a wall of opposite chirality partially destroys selectivity. Recently it has been claimed that in isolated Y-shaped junctions that support vortex walls, selectivity is entirely determined by chirality (or topology), the suggestion being that vortex wall chirality is robust in the Walker breakdown process. Here we demonstrate that in Y-shaped junctions, magnetic switching in the important topologically protected regime exists only for a narrow window of field and bar geometry, and that it will be challenging to access this regime in field-driven ASI. This work has implications for the wider field of magnetic charge manipulation for high density memory storage.

Introduction

Artificial spin ice (ASI) arrays of ferromagnetic nanobars are frustrated systems whose dimensions can be chosen to facilitate the direct imaging of individual nanobar magnetization [1, 2]. The shape anisotropy of each nanobar forces its magnetization to lie in one of two directions along its long axis and so it acts as an 'ising macrospin'. The term ASI was originally applied to a square array of electrically and magnetically isolated bars [3], but here we consider continuous honeycomb or kagome ASI structures [4–16]. In the honeycomb three of these ising macrospins meet at each vertex and their interactions are governed by a set of 'ice rules', which minimize the local magnetic charge at each vertex without favouring a specific spin structure. Thus, as long as each wire is magnetized along its ising axis, the magnetic energy of an ASI array depends only upon magnetic charge distribution and not on the spin structure. If all of the dipoles in the lattice are of the same size and have the same magnetic moment, then the magnetic charge in the lattice is quantized into multiples of $q = m/l$, in which m is the dipole moment and l is the dipole length. A consequence of this exotic magnetic ordering principle is that there is no magnetic energy cost to move magnetic charges around the lattice [17]. Thus the defects are 'quasiparticles', act as magnetic charge carriers and are sometimes known as 'magnetic monopoles'. This is very attractive as a method of manipulating data, particularly if the charges can be routed controllably through junctions.

For ferromagnetic nanowires of the dimensions considered here magnetic reversal occurs by the motion of a domain wall from one end of the wire to the other, and it is these domain walls that carry the magnetic charge. In connected ASI structures the nucleation field (H_N) required to nucleate domain walls at an arbitrary position
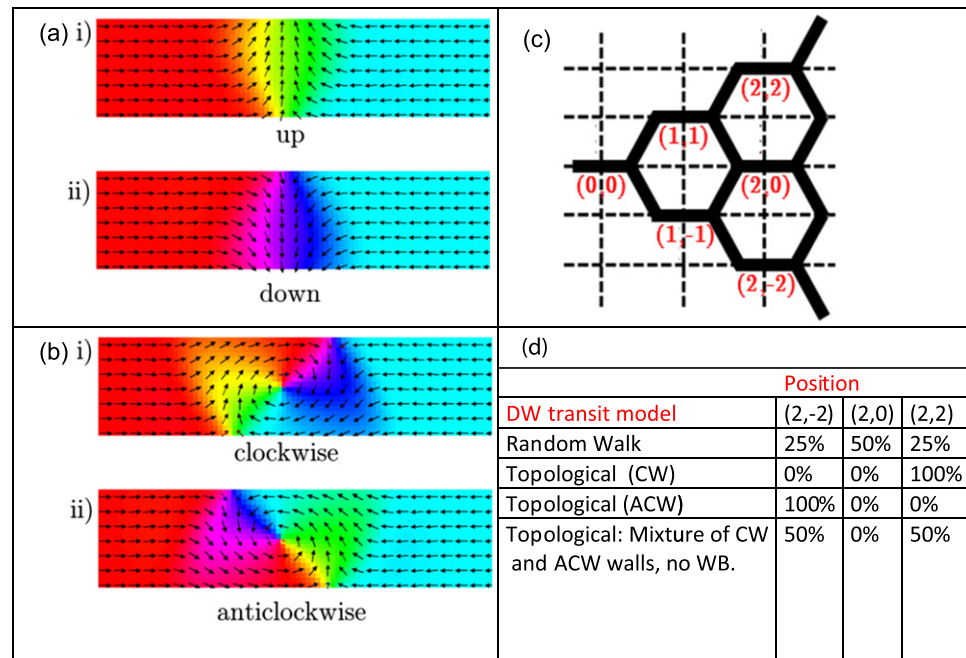
Figure 1. Micromagnetic simulations showing (a) transverse (i) up chirality and (ii) down chirality and (b) vortex (i) clockwise chirality and (ii) anticlockwise chirality head-to-head domain walls. The simulations were performed using the OOMMF software [18] for permalloy with mesh size [5 nm, 5 nm, 10 nm] and nanowire dimensions of (a) 1000 nm × 100 nm × 10 nm and (b) 1000 nm × 100 nm × 40 nm. (c) Schematic of labelling of sites in a DW transit path. (d) expected probability distribution of domain wall position for different DW transit models.

within the lattice is significantly greater than both the nucleation field at an edge site and the propagation field (H_P) required to transmit a pre-existing domain wall down a nanobar. Thus the majority of the bars in the array switch by edge nucleation and subsequent propagation of a small number of domain walls [10, 12]. The observed switching fields are well described by H_P, as predicted from a simple model whereby the domain wall is treated as a uniform ball of magnetic charge moving under the influence of a uniform external magnetic field and Coulombic interactions with additional trapped magnetic charges at each vertex [7–9]. If the magnetic field axis is parallel to one of the sublattice directions then the propagating charge will repeatedly arrive at Y-shaped junctions with bar angle $\theta = 120°$ where it is forced to select between two apparently equivalent paths. However, there is the potential to break the symmetry of this decision because domain walls in in-plane magnetized nanobars are more complex, adopting for example transverse or vortex micromagnetic structures (see figures 1(a) and (b)). The most energetically favoured structure depends on the nanobar dimensions, but both wall types are chiral objects with two energetically equivalent configurations of opposite chirality. In the simplest transit model one would expect the domain wall to take the upward and downward paths with equal probability and hence execute a random walk. This would produce a distribution of propagation paths as explained in figures 1(c) and (d). A biased random walk (closer to the topological model with walls of both chirality and no Walker breakdown shown in figures 1(c) and (d)) was observed in previous studies of domain wall trajectories in permalloy ASIs in the transverse domain wall regime [15]. The strong, although far from perfect, selectivity [15, 16] came from the chirality breaking the symmetry at the vertex and the continued element of randomness from the loss of chiral fidelity due to Walker breakdown [18].

In permalloy nanowires, as the cross-section of the wire diminishes there is a crossover from vortex DW to transverse DW behaviour at a total cross-section of around 2000 nm^2 [19, 20]. In typical ASI structures [6, 11, 13] the bar width is around 100–200 nm, and so the crossover occurs at a thickness of around 20 nm. Recently, perfect selectivity was demonstrated in Y-shaped permalloy junctions with a much smaller angle ($\theta = 45°$, 60°) between the possible paths and it was proposed [21] that this perfect selectivity could be extended to ASIs in the vortex wall regime because the direction of propagation is topologically protected. Path selection is controlled by vortex chirality as in the transverse wall case, specifically the leading topological edge defect of the vortex wall, and the topological protection relies on vortex chirality being robust under Walker breakdown [22]. However, it has been predicted that this is only the lowest energy mode of Walker breakdown and at a slightly higher field (H_2) a second mode associated with the emission of an antivortex from one of the edge defects becomes significant [22], and eventually Walker breakdown with reversal of vortex chirality becomes possible [23]. The topological control mode is very attractive, both as a controllable switch in domain-wall type logic

devices [24] and as a route to writing specific magnetic microstates into ASI arrays for novel types of computation or forming monopole defects [12] at defined locations. Thus it is important to map out the parameter space in detail for this type of junction. At small θ (e.g. $\theta = 20°$) cloning [25] (nucleation in both branches) occurs rather than selective transit across the junction. From a simple geometric approximation [9] that in a nanowire with ising anisotropy the magnetic force driving a domain wall down the nanowire will be proportional to the resolved component of the magnetic field in the wire direction, we argue that the transit field will increase as $\cos(\theta/2)$ and so at large θ, such as $120°$ in ASI, the transit field is likely to exceed H_2. Thus we have a reliable logic function based on the spin texture of the DW as it arrives at the Y-shaped junction, but it is unclear to what extent this chiral spin texture can be conserved while moving DWs in ASI nanostructures.

Here we address this point using micromagnetic simulations and direct imaging of DW trajectories in an ASI structure. The experimental structures have wire thickness 36 nm and width near 180 nm to ensure that we are well within the vortex DW regime. Our micromagnetic simulations show that in our structures and other standard vortex DW ASI structures (with $\theta = 120°$), H_P exceeds H_2 and therefore that we are unable to access the topologically protected regime [21]. This is consistent with our imaging experiments, where we find that there is no strong correlation between propagation directions at neighbouring vertices. In fact from our statistical data we are not able to reject the random walk hypothesis in our experimental structures at a 5% confidence level.
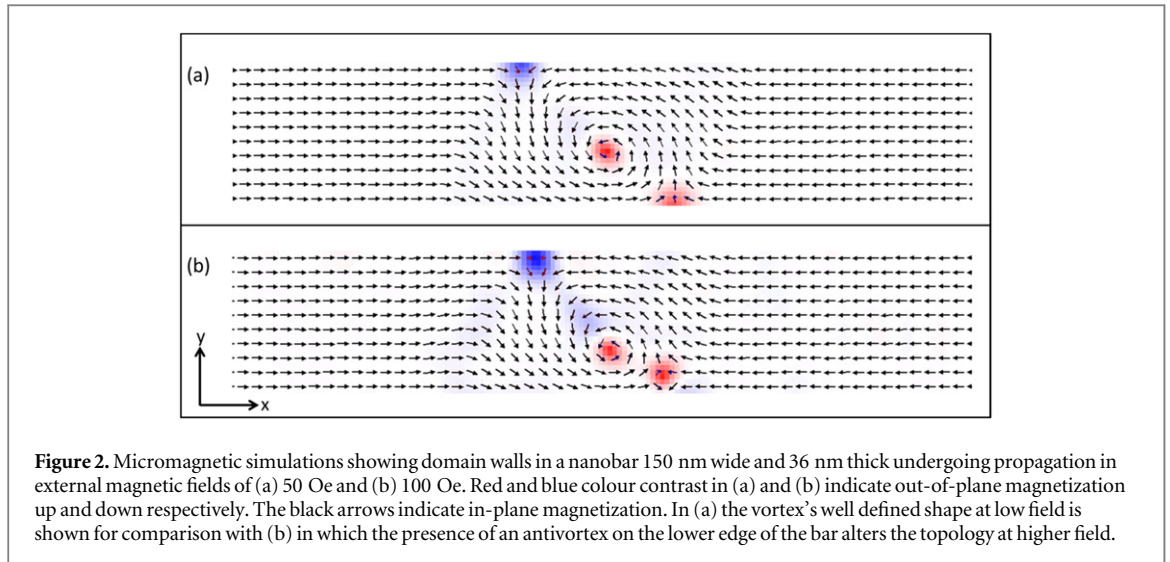
Method

ASI arrays comprising 21×19 honeycombs were structured from permalloy, $Ni_{81}Fe_{19}$, onto x-ray transparent SiN windows using an electron beam lithography, thermal evaporation and lift-off processing technique. Two different ASI arrays of nanobar dimensions $1.5\ \mu m \times 173 \pm 10\ nm \times 36\ nm$ and $2\ \mu m \times 181 \pm 5\ nm \times 36\ nm$ were fabricated. The nanobars in these arrays are well within the vortex wall regime according to our simulations and previous studies [19, 20, 26]. The magnetization was studied as a function of in-plane field using room temperature scanning transmission x-ray microscopy (STXM) at beamline 11.02 of the Advanced Light Source (Berkeley, CA, USA). The sample was mounted between the pole pieces of an electromagnet allowing the application of an in-plane field of $\pm 250\ mT$ *in situ*. The chamber was pumped down to a pressure of approximately 100 mTorr before filling with He gas. Elliptically polarized x-rays were provided by an undulator beamline after which they were focused to a spot size of approximately 30 nm using a Fresnel zone plate. The in-plane component of the magnetization was probed using the x-ray magnetic circular dichroism effect by mounting the sample and the electromagnet approximately $30°$ with respect to the x-ray propagation vector. In order to study the magnetization reversal of the array, the sample was first saturated in one field direction, and then a small field was applied in the opposite field direction and increased incrementally allowing for the acquisition of STXM images at remanence after each field step. Image analysis and statistical correlations between two sequential decisions made by a domain wall at a Y-shaped junction were investigated as in the previous work on ASI in the transverse domain wall regime [15].

Micromagnetic simulations were performed using the Object Oriented Micromagnetic Framework (OOMMF) to aid the interpretation of the experimental results [27]. The simulations are at absolute zero temperature. Mesh sizes of [5 nm, 5 nm, 9 nm] were used in all simulations. The exchange constant and saturation magnetization for permalloy were taken to be $13 \times 10^{-12}\ J\ m^{-1}$ and $800\ kA\ m^{-1}$ respectively. The Gilbert damping parameter was taken to be $\alpha = 0.01$. Preconditioned initial states were used with magnetization in the negative x-direction and with a domain wall included in the horizontal arm. This enabled the study of all four possible chirality–polarity permutations (polarity describes direction of the vortex core, up or down). These preconditioned domain walls were subsequently driven by an external field in the positive x-direction and the magnetization configuration was recorded every 0.09 ns.

Results and discussion

Let us start by reviewing what is understood about a vortex domain wall moving along a bar in a fixed field H. Figure 2 shows a typical snapshot of the micromagnetic structure of an initial anticlockwise chirality, up polarity, domain wall as it propagates through a 150 nm wide, 36 nm thick nanobar under the influence of external axial magnetic fields of magnitudes 50 Oe and 100 Oe. Videos of the full propagation simulations at 50 Oe, 100 Oe, 200 Oe, 300 Oe, 400 Oe and 500 Oe are included in the supplemental material. At 50 Oe, conservation of domain wall chirality but change of polarity was seen during propagation which is consistent with lowest energy mode Walker breakdown [22] required for the topologically protected regime [21]. In addition the vortex domain wall had a well-defined shape, an example of which is shown in figure 2(a). However at 100 Oe, although the vortex domain wall's chirality was robust, its shape became more complex and the emission of an antivortex from the lower edge (figure 2(b)) altered the topology. This emission of an antivortex from the leading

Figure 2. Micromagnetic simulations showing domain walls in a nanobar 150 nm wide and 36 nm thick undergoing propagation in external magnetic fields of (a) 50 Oe and (b) 100 Oe. Red and blue colour contrast in (a) and (b) indicate out-of-plane magnetization up and down respectively. The black arrows indicate in-plane magnetization. In (a) the vortex's well defined shape at low field is shown for comparison with (b) in which the presence of an antivortex on the lower edge of the bar alters the topology at higher field.
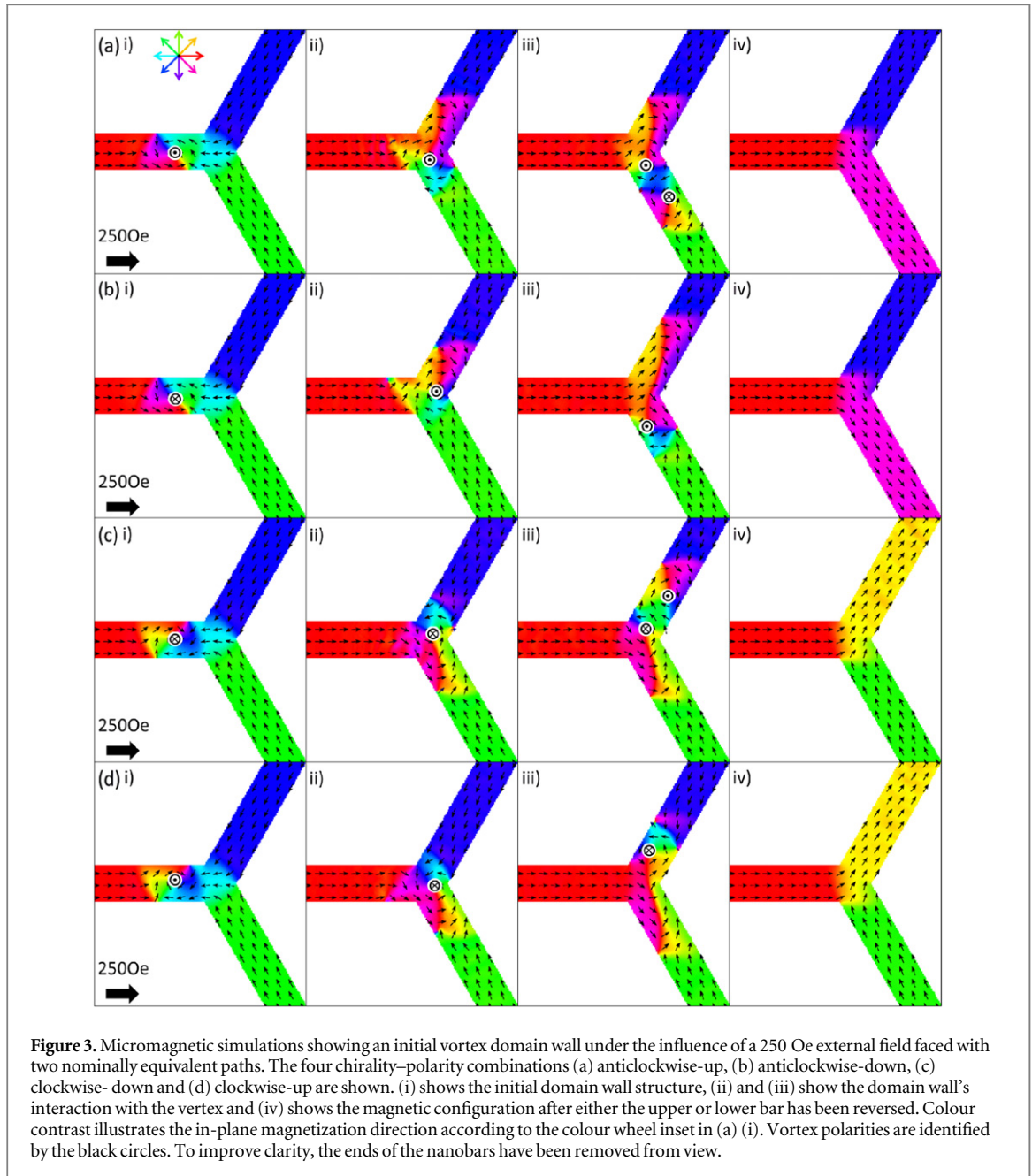
topological edge defect, with concomitant change of sign of the topological charge of the edge defect is the second Walker mode excitation identified above H_2 by Tretiakov *et al* [22]. As the edge topological charge underpins the topological selectivity we can no longer anticipate perfect selectivity at fields of 100 Oe or more. In fact the field at which this mode plays some role in the dynamics of the system (H_2) was found [22] to be 35 Oe, so there is doubt about the topological protection above this field, although we do not directly observe the antivortices in the 50 Oe simulations of our specific geometry. Furthermore, at 500 Oe Walker breakdown with a reversal of vortex chirality was observed [23]. In light of the field-induced domain wall transformations described above it is clear that the magnetic field required to switch our structures, of around 100 Oe, places us in a different regime of uncertain selectivity.
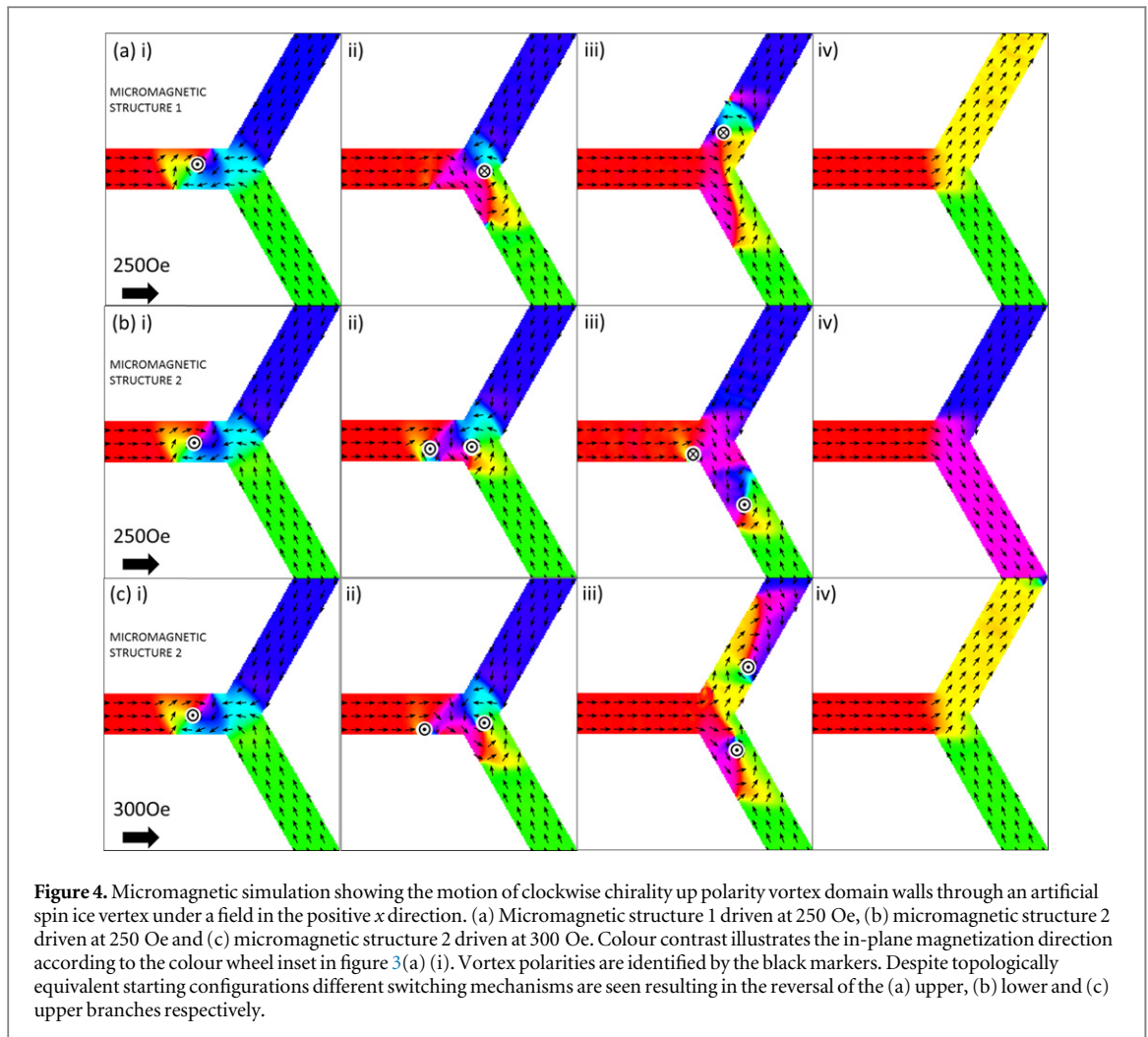
Now let us examine the situation in a Y-shaped junction composed of 150 nm wide, 36 nm thick bars and $\theta = 120°$ i.e. an isolated ASI vertex. Figure 3 shows micromagnetic simulations of all four chirality polarity permutations in an applied field of 250 Oe. An initial vortex domain wall structure was introduced to the left of the vertex and allowed to evolve in an external magnetic field. Initial anticlockwise chirality domain walls of both up and down polarities resulted in the lower branch's reversal (figures 4(a) and (b)) and initial clockwise chirality domain walls of both up and down polarities resulted in the upper branch's reversal (figures 4(c) and (d)). These findings are consistent with a purely topological model of domain wall trajectory [21]. However, the variations between our observed states in part (iii) of figures 3(a)–(d) and Pushp *et al* [21] raise questions about the robustness of the mechanism.

Figure 4 shows the outcome of simulations similar to those shown in figure 3, but with small permutations of vortex starting configuration and applied field. Two different starting configurations were used which we shall call 'micromagnetic structure 1' (which is identical to the starting configuration used in figure 3(d)) and 'micromagnetic structure 2' in which the starting position of the vortex core has changed by 25 nm. Figure 4(a) shows the propagation of micromagnetic structure 1 under 250 Oe (identical to figure 3(d)) resulting in the reversal of the upper branch and figure 4(b) shows the propagation of micromagnetic structure 2 under 250 Oe resulting in the reversal of the lower branch. From these simulations it is clear that two domain walls of identical chirality and polarity (and hence topology), but slightly different specific micromagnetic structure, driven at the same external field can result in the switching of different branches. In addition it was seen that two domain walls, identical in terms of topology and micromagnetics, driven at different fields resulted in the switching of different branches. The propagation of micromagnetic structure 2 at 250 Oe, resulting in the reversal of the lower branch, is shown in figure 4(b), and at 300 Oe, resulting in the reversal of the upper branch, is shown in figure 4(c). These simulations clearly demonstrate that in this regime we can set up a specific experiment that gives chiral path selectivity, but that a small perturbation to the vortex starting position and the drive field, which do not affect the topology, can reverse the selected direction for all four chirality and polarity permutations. The sign change in the selectivity is likely to be a signature of periodic oscillatory behaviour at a frequency [16, 28, 29] controlled by the applied field. As it is also clear that at the fields we are using the topology of the vortex domain wall is not protected, the lack of selectivity in our experiments is unsurprising.

As the Walker breakdown critical fields decrease with increasing temperature [30] it is possible that, at room temperature we are in an even more complex regime than that shown in our zero temperature simulations in figure 3(b). Let us now see how finite temperature measurements compare with these zero temperature simulations. Figure 5(a) shows a typical STXM image during the field-driven magnetic reversal of ASI taken at

Figure 3. Micromagnetic simulations showing an initial vortex domain wall under the influence of a 250 Oe external field faced with two nominally equivalent paths. The four chirality–polarity combinations (a) anticlockwise-up, (b) anticlockwise-down, (c) clockwise- down and (d) clockwise-up are shown. (i) shows the initial domain wall structure, (ii) and (iii) show the domain wall's interaction with the vertex and (iv) shows the magnetic configuration after either the upper or lower bar has been reversed. Colour contrast illustrates the in-plane magnetization direction according to the colour wheel inset in (a) (i). Vortex polarities are identified by the black circles. To improve clarity, the ends of the nanobars have been removed from view.
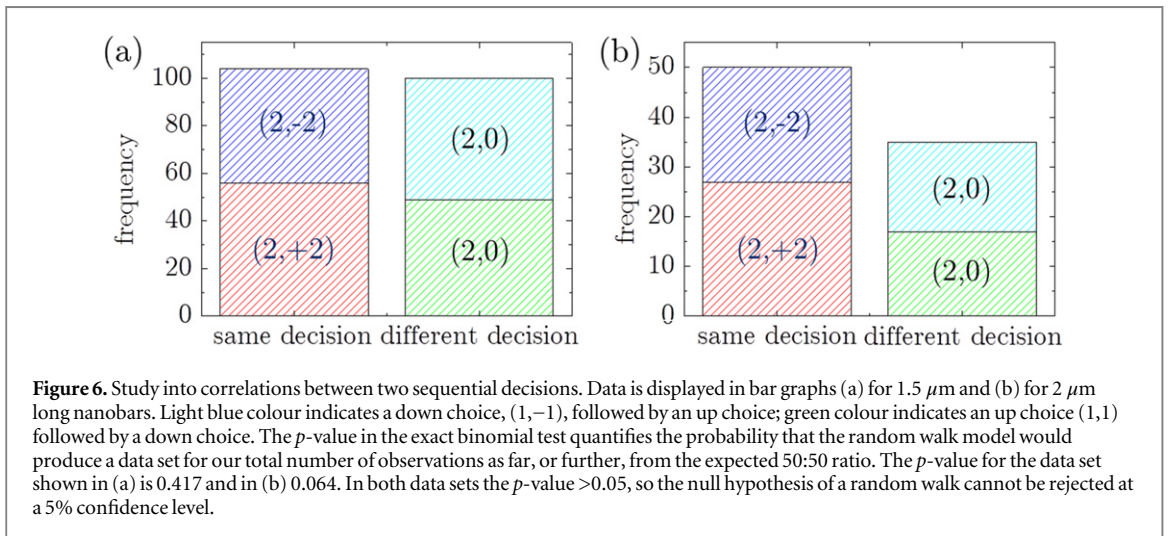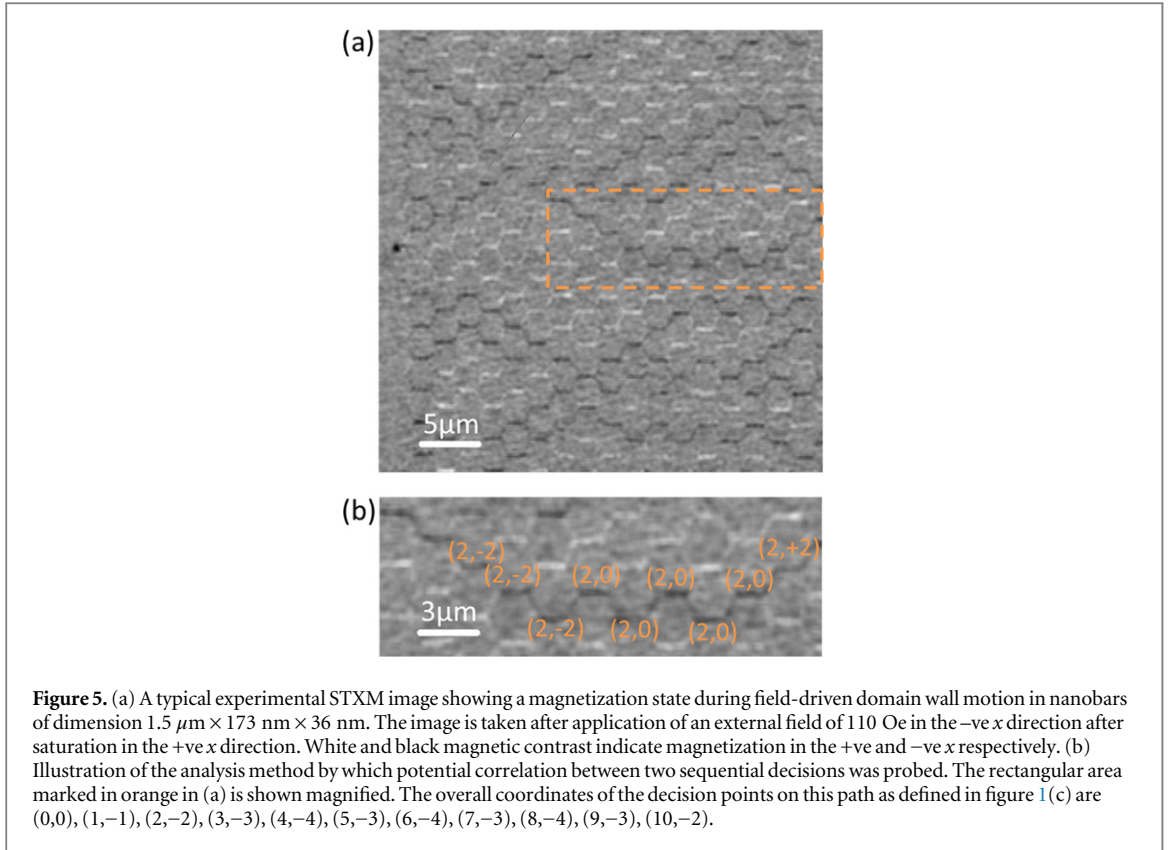
remanence and at room temperature. The black reversed nanobars indicate the paths through which domain walls have propagated. In this image the external field has been stepped up to 110 Oe, and it is clear that magnetic reversal is far from complete at this field. Correlations between two sequential decisions made by a domain wall at a Y-shaped junction were investigated. The number of incidences in which the domain wall chose the upper branch followed by the upper branch, the upper branch followed by the lower branch, the lower branch followed by the upper branch and the lower branch followed by the lower branch were counted. This method for analysis of two sequential decisions is illustrated in figure 5(b). A summary of the statistical correlations between sequential vertices is shown in figure 6. For 1.5 μm long nanobars, from 204 events, domain walls made the same decision twice 104 times and two different decisions 100 times. This is strikingly close to the expected ratio for a random walk (figures 1(c) and (d)) where there is no correlation between two sequential decisions. An exact binomial test of the random walk hypothesis performed on this data yielded a *p*-value of 0.417. This *p*-value quantifies the probability that the random walk model would produce a data set for our number of total observations as far, or further, from the expected 50:50 ratio. This result therefore suggests that, for nanobar dimensions 1.5 μm $\times$ 173 nm $\times$ 36 nm, domain walls do indeed exhibit a random walk. This result differs starkly from our previous observation [15] that for ASI structures where we have transverse domain walls (nanobars of dimension 100 nm $\times$ 1 μm $\times$ 18 nm) a random walk situation is exceptionally unlikely, with an equivalent *p*-value of 1.7×10^{-9}. For 2 μm long nanobars we have fewer observations; from 85 events, domain walls made the

Figure 4. Micromagnetic simulation showing the motion of clockwise chirality up polarity vortex domain walls through an artificial spin ice vertex under a field in the positive *x* direction. (a) Micromagnetic structure 1 driven at 250 Oe, (b) micromagnetic structure 2 driven at 250 Oe and (c) micromagnetic structure 2 driven at 300 Oe. Colour contrast illustrates the in-plane magnetization direction according to the colour wheel inset in figure 3(a) (i). Vortex polarities are identified by the black markers. Despite topologically equivalent starting configurations different switching mechanisms are seen resulting in the reversal of the (a) upper, (b) lower and (c) upper branches respectively.

same decision twice 50 times and two different decisions 35 times. This result is illustrated in figure 6(b). The equivalent exact binomial test of the random walk hypothesis performed on this data yielded a *p*-value of 0.064. Although this *p*-value is considerably lower than the value achieved for 1.5 μm bars, the null-hypothesis of a random walk is still accepted if a 5% significance level is applied.

The control of vortex type and selectivity of transit direction demonstrated by Pushp *et al* [21] would be highly desirable for logic type operations in ASI structures, so we now consider the prospects for accessing the perfectly selective regime in ASI. The operating field window for any sort of logic function in ASI requires that targeted domain wall nucleation and the ice rules enable the reversal of selected bars by controlled propagation whilst the remaining bars are unaffected. In our current experimental structure this operating window is centred on approximately 110 Oe, which is well above the H_2 field where the topological protection is lost. This operating field, dependent on the domain wall nucleation and depinning fields within the structure is a function of nanobar dimensions, and the angle of opening between the non-horizontal nanobars ($\cos(\theta/2)$). That perfect fidelity has been demonstrated experimentally at $\theta = 45°$ and $H = 55$ Oe by Pushp *et al* [21] shows that only a factor of 2 reduction in operating field ($[\cos(22.5°)/\cos(60°)]$) is needed for ASI to be in the topologically protected regime if the Pushp and Phung sample wire dimensions are taken as a starting point. In principle this reduction can be obtained by changing the constituent materials, bar dimensions or edge features, but the parameter space is rather complex as manipulations to reduce the transit field are also likely to affect the domain wall phase diagram and stability. A natural strategy is reducing the volume and decreasing the aspect ratio of the bars' cross-section [31] (t/w), although these changes have potential implications for the domain wall type and Walker breakdown mechanism. Permalloy is the softest available bulk crystalline ferromagnetic material, but the use of amorphous ferromagnetic alloys or ultrathin films could provide another route to reduced operating fields [32, 33]. Disconnected ASI structures have recently been fabricated from amorphous alloys [34] and monolayer iron embedded in palladium [35]. Connected structures from these materials merit exploration, although again there will be implications for the domain wall behaviour. In these amorphous materials, as in their crystalline counterparts, edge features can play an important role in domain wall nucleation and pinning

Figure 5. (a) A typical experimental STXM image showing a magnetization state during field-driven domain wall motion in nanobars of dimension 1.5 μm $\times$ 173 nm $\times$ 36 nm. The image is taken after application of an external field of 110 Oe in the $-$ve x direction after saturation in the $+$ve x direction. White and black magnetic contrast indicate magnetization in the $+$ve and $-$ve x respectively. (b) Illustration of the analysis method by which potential correlation between two sequential decisions was probed. The rectangular area marked in orange in (a) is shown magnified. The overall coordinates of the decision points on this path as defined in figure 1(c) are $(0,0)$, $(1,-1)$, $(2,-2)$, $(3,-3)$, $(4,-4)$, $(5,-3)$, $(6,-4)$, $(7,-3)$, $(8,-4)$, $(9,-3)$, $(10,-2)$.

Figure 6. Study into correlations between two sequential decisions. Data is displayed in bar graphs (a) for 1.5 μm and (b) for 2 μm long nanobars. Light blue colour indicates a down choice, $(1,-1)$, followed by an up choice; green colour indicates an up choice $(1,1)$ followed by a down choice. The *p*-value in the exact binomial test quantifies the probability that the random walk model would produce a data set for our total number of observations as far, or further, from the expected 50:50 ratio. The *p*-value for the data set shown in (a) is 0.417 and in (b) 0.064. In both data sets the *p*-value $>$0.05, so the null hypothesis of a random walk cannot be rejected at a 5% confidence level.

fields [36], so it may also be possible to reduce the pinning strength by tailoring the vertex shape to remove sharp corners. Thus, there are still challenges to be overcome before a truly topologically protected ASI can be realised, but there are a number of promising avenues which merit further exploration.

In summary, micromagnetic simulations of the magnetic switching of Y-shaped junctions suggest that the topology of the wall at the point of transit controls the path. However, at the fields required to switch our structures in the simulations, the topological information is not reliably conserved between vertices. This is consistent with our room temperature observations of the field-driven trajectories of the vortex domain walls in connected ASI structures using STXM. Our statistical data show that the transit is certainly not perfectly selective and in fact we are unable to reject the random walk hypothesis at a 5% confidence level. These findings show that careful optimization of the ASI geometry is required to achieve topological control of the path. Understanding the limitations of by these path selection rules for the vortex domain wall regime fully is essential for domain wall

memory and processing applications [37, 38], manipulation of magnetic nanoparticles [39–42] and the manipulation of cold atoms [43].

Acknowledgments

References

[1] Nisoli C, Moessner R and Schiffer P 2013 Colloquium: artificial spin ice: designing and imaging magnetic frustration *Rev. Mod. Phys.* **85** 1473–90

[2] Heyderman L J and Stamps R L 2013 Artificial ferroic systems: novel functionality from structure, interactions and dynamics *J. Phys.: Condens. Matter* **25** 363201

[3] Wang R F *et al* 2006 Artificial 'spin ice' in a geometrically frustrated lattice of nanoscale ferromagnetic islands *Nature* **439** 303–6

[4] Tanaka M, Saitoh E, Miyajima H, Yamaoka T and Iye Y 2005 Domain structures and magnetic ice-order in NiFe nano-network with honeycomb structure *J. Appl. Phys.* **97** 10J710

[5] Tanaka M, Saitoh E, Miyajima H, Yamaoka T and Iye Y 2006 Magnetic interactions in a ferromagnetic honeycomb nanoscale network *Phys. Rev.* B **73** 052411

[6] Qi Y, Brintlinger T and Cumings J 2008 Direct observation of the ice rule in an artificial kagome spin ice *Phys. Rev.* B **77** 094418

[7] Ladak S, Read D E, Perkins G K, Cohen L F and Branford W R 2010 Direct observation of magnetic monopole defects in an artificial spin-ice system *Nat. Phys.* **6** 359–63

[8] Tchernyshyov O 2010 Magnetic monopoles—no longer on thin ice *Nat. Phys.* **6** 323–4

[9] Mellado P, Petrova O, Shen Y C and Tchernyshyov O 2010 Dynamics of magnetic charges in artificial spin ice *Phys. Rev. Lett.* **105** 187206

[10] Ladak S, Read D E, Branford W R and Cohen L F 2011 Direct observation and control of magnetic monopole defects in an artificial spin-ice material *New J. Phys.* **13** 063032

[11] Daunheimer S A, Petrova O, Tchernyshyov O and Cumings J 2011 Reducing disorder in artificial kagome ice *Phys. Rev. Lett.* **107** 167201

[12] Ladak S, Read D, Tyliszczak T, Branford W R and Cohen L F 2011 Monopole defects and magnetic Coulomb blockade *New J. Phys.* **13** 023023

[13] Ladak S, Walton S K, Zeissler K, Tyliszczak T, Read D E, Branford W R and Cohen L F 2012 Disorder-independent control of magnetic monopole defect population in artificial spin-ice honeycombs *New J. Phys.* **14** 045010

[14] Branford W R, Ladak S, Read D E, Zeissler K and Cohen L F 2012 Emerging chirality in artificial spin ice *Science* **335** 1597–600

[15] Zeissler K, Walton S K, Ladak S, Read D E, Tyliszczak T, Cohen L F and Branford W R 2013 The non-random walk of chiral magnetic charge carriers in artificial spin ice *Sci. Rep.-Uk* **3** 1252

[16] Burn D M, Chadha M, Walton S K and Branford W R 2014 Dynamic interaction between domain walls and nanowire vertices *Phys. Rev.* B **90** 144414

[17] Castelnovo C, Moessner R and Sondhi S L 2008 Magnetic monopoles in spin ice *Nature* **451** 42–5

[18] Schryer N L and Walker L R 1974 Motion of 180 degrees domain-walls in uniform dc magnetic-fields *J. Appl. Phys.* **45** 5406–21

[19] Nakatani Y, Thiaville A and Miltat J 2005 Head-to-head domain walls in soft nano-strips: a refined phase diagram *J. Magn. Magn. Mater.* **290** 750–3

[20] McMichael R D and Donahue M J 1997 Head to head domain wall structures in thin magnetic strips *IEEE Trans. Magn.* **33** 4167–9

[21] Pushp A, Phung T, Rettner C, Hughes B P, Yang S H, Thomas L and Parkin S S P 2013 Domain wall trajectory determined by its fractional topological edge defects *Nat. Phys.* **9** 505–11

[22] Tretiakov O A, Clarke D, Chern G W, Bazaliy Y B and Tchernyshyov O 2008 Dynamics of domain walls in magnetic nanostrips *Phys. Rev. Lett.* **100** 127204

[23] Lee J Y, Lee K S, Choi S, Guslienko K Y and Kim S K 2007 Dynamic transformations of the internal structure of a moving domain wall in magnetic nanostripes *Phys. Rev.* B **76** 184408

[24] Parkin S S P, Hayashi M and Thomas L 2008 Magnetic domain-wall racetrack memory *Science* **320** 190–4

[25] Allwood D A, Xiong G and Cowburn R P 2007 Domain wall cloning in magnetic nanowires *J. Appl. Phys.* **101** 024308

[26] Klaui M, Vaz C A F, Bland J A C, Heyderman L J, Nolting F, Pavlovska A, Bauer E, Cherifi S, Heun S and Locatelli A 2004 Head-to-head domain-wall phase diagram in mesoscopic ring magnets *Appl. Phys. Lett.* **85** 5637–9

[27] Donahve M J and Porter D G 1999 *OOMMF User's Guide* version 1.0 (National Institute of Standards and Technology, Gaithersburg, MD)

[28] Thiaville A, Garcia J M and Miltat J 2002 Domain wall dynamics in nanowires *J. Magn. Magn. Mater.* **242** 1061–3

[29] Beach G S D, Nistor C, Knutson C, Tsoi M and Erskine J L 2005 Dynamics of field-driven domain-wall propagation in ferromagnetic nanowires *Nat. Mater.* **4** 741–4

[30] Yang J 2013 Study of static spin distributions and dynamics of magnetic domn walls in soft magnetic nanostructures *PhD Thesis* University of Texas

[31] Uhlig W C and Shi J 2004 Systematic study of the magnetization reversal in patterned Co and NiFe nanolines *Appl. Phys. Lett.* **84** 759–61

[32] Gavrila H and Ionita V 2002 Crystalline and amorphous soft magnetic materials and their applications—status of art and challenges *J. Optoelectron. Adv. Mater.* **4** 173–91

[33] McHenry M E, Willard M A and Laughlin D E 1999 Amorphous and nanocrystalline materials for applications as soft magnets *Prog. Mater. Sci.* **44** 291–433

[34] Montaigne F *et al* 2014 Size distribution of magnetic charge domains in thermally activated but out-of-equilibrium artificial spin ice *Sci. Rep. UK* **4** 5702

[35] Kapaklis V, Arnalds U B, Harman-Clarke A, Papaioannou E T, Karimipour M, Korelis P, Taroni A, Holdsworth P C W, Bramwell S T and Hjorvarsson B 2012 Melting artificial spin ice *New J. Phys.* **14** 035009

[36] Schafer R, Ho W K, Yamasaki J, Hubert A and Humphrey F B 1991 Anisotropy pinning of domain-walls in a soft amorphous magnetic material *IEEE Trans. Magn.* **27** 3678–89

[37] Hayashi M, Thomas L, Moriya R, Rettner C and Parkin S S P 2008 Current-controlled magnetic domain-wall nanowire shift register *Science* **320** 209–11

[38] Allwood D A, Xiong G, Faulkner C C, Atkinson D, Petit D and Cowburn R P 2005 Magnetic domain-wall logic *Science* **309** 1688–92

[39] Donolato M *et al* 2010 On-chip manipulation of protein-coated magnetic beads via domain-wall conduits *Adv. Mater.* **22** 2706

[40] Vavassori P, Gobbi M, Donolato M, Cantoni M, Bertacco R, Metlushko V and Ilic B 2010 Magnetic nanostructures for the manipulation of individual nanoscale particles in liquid environments (invited) *J. Appl. Phys.* **107** 09B301

[41] Rapoport E and Beach G S D 2012 Dynamics of superparamagnetic microbead transport along magnetic nanotracks by magnetic domain walls *Appl. Phys. Lett.* **100** 082401

[42] Ruan G, Vieira G, Henighan T, Chen A R, Thakur D, Sooryakumar R and Winter J O 2010 Simultaneous magnetic manipulation and fluorescent tracking of multiple individual hybrid nanostructures *Nano Lett.* **10** 2220–4

[43] West A D, Weatherill K J, Hayward T J, Fry P W, Schrefl T, Gibbs M R J, Adams C S, Allwood D A and Hughes I G 2012 Realization of the manipulation of ultracold atoms with a reconfigurable nanomagnetic system of domain walls *Nano Lett.* **12** 4065–9